

Magnetically induced current densities in Al_4^{2-} and Al_4^{4-} species studied at the coupled-cluster level

Ying-Chan Lin, Jonas Jusélius, and Dage Sundholm^{a)}

Department of Chemistry, University of Helsinki, P.O. Box 55 (A.I. Virtanens plats 1),
FIN-00014 Helsinki, Finland

Jürgen Gauss

Institut für Physikalische Chemie, Universität Mainz, Jakob-Welder Weg 11, D-55099 Mainz, Germany

(Received 15 March 2005; accepted 6 April 2005; published online 6 June 2005)

Magnetically induced current densities in the four-membered rings of Al_4^{2-} and Al_4^{4-} species have been calculated at the coupled-cluster singles and doubles (CCSD) level by applying the recently developed gauge-including magnetically induced current (GIMIC) method. The strength of the ring-current susceptibilities were obtained by numerical integration of the current densities passing through a cross section perpendicular to the Al_4 ring. The GIMIC calculations support the earlier notion that Al_4^{2-} with formally two π electrons sustains a net diatropic ring current. The diatropic contribution to the ring-current susceptibility is carried by the electrons in both the σ (16.7 nA/T) and the π (11.3 nA/T) orbitals. The induced ring current in the Al_4^{4-} compounds, with four π electrons, consists of about equally strong diatropic σ and paratropic π currents of about 14 and -17 nA/T, respectively. The net current susceptibilities obtained for Al_4Li^- , Al_4Li_2^- , Al_4Li_3^- , and Al_4Li_4^- at the CCSD level using a triple-zeta basis set augmented with polarization functions are 28.1, 28.1, -5.9 , and -3.1 nA/T, respectively. The corresponding diatropic (paratropic) contributions to the ring-current susceptibilities are 32.4 (0.0), 36.7 (0.0), 18.9 (-19.9), and 18.6 (-16.8) nA/T, respectively. For the Al_4^{2-} and Al_4^{4-} species, the net currents circling each Li^+ cation is estimated to 4.3 and 2.4 nA/T, respectively. © 2005 American Institute of Physics.
[DOI: 10.1063/1.1924590]

I. INTRODUCTION

Ring-shaped aluminum species consisting of four aluminum atoms have recently been studied experimentally in laser vaporization experiments using photoelectron spectroscopy.^{1,2} The experimental results were interpreted by employing *ab initio* and density-functional theory (DFT) calculations. The calculations showed that the geometry of the Al_4^{2-} cluster is square shaped with equal Al–Al bonds. The Al_4^{2-} compounds have two delocalized π electrons, indicating that they are aromatic according to Hückel's $(4n+2)\pi$ rule.¹ In later experiments, Kuznetsov *et al.*² were able to vaporize reduced ring-shaped aluminum clusters consisting of four Al atoms and to detect Al_4^{4-} species. Their computational studies showed that the 4π Al_4^{4-} species form an aluminum ring with alternating Al–Al bonds, suggesting that they are antiaromatic similarly as cyclobutadiene.

A DFT study of the magnetic shielding properties of Al_4^{4-} by Chen *et al.*³ did not completely support this notion; instead nucleus-independent chemical shift⁴ (NICS) calculations indicated that Al_4^{4-} can be classified as a σ -aromatic and π -antiaromatic species. Fowler and co-workers^{5,6} calculated magnetically induced currents at the Hartree–Fock self-consistent-field (HF SCF) level. The current-density plots showed that both Al_4^{2-} and Al_4^{4-} sustain diatropic current densities in the Al_4 plane; this was taken as a clear indication of

the σ aromaticity of the aluminum four-membered rings.^{5,6} For Al_4^{2-} , Fowler and co-workers did not obtain any ring-current density in regions which are 1 bohr and higher above the aluminum-ring plane, whereas for Al_4Li_4 they found strong paratropic currents in a plane 2 bohrs above the aluminum atoms. Thus, according to their calculations, the π orbital in Al_4^{2-} is magnetically inactive, whereas in the Al_4^{4-} species, they found that the π cloud sustains a net paratropic current. The calculated current-density maps by Fowler and co-workers^{5,6} support the notion that Al_4^{2-} can be considered to be σ aromatic and that Al_4^{4-} is a σ -aromatic and π -antiaromatic species.

Thus, according to the previous studies, NICS values and current-density plots indicated that the Al_4^{2-} and Al_4^{4-} rings sustain net diatropic ring currents suggesting that they are both aromatic. On the other hand, the formal π -electron count and the molecular structures suggest that the Al_4^{2-} species are aromatic and that the Al_4^{4-} ring constitutes an antiaromatic metal cluster. This contradiction shows that the aromatic properties of the Al_4 rings are very tantalizing (for a recent discussion, see also Ref. 7, for other computational studies concerning the aromaticity/antiaromaticity of Al_4 species, see Refs. 8–15) and a more thorough study is needed to sort out this conundrum.

In this work, we resolve this problem by calculating the magnetically induced current densities and nuclear magnetic shieldings for the Al_4^{2-} and Al_4^{4-} species at the coupled-cluster level as well as by employing density-functional

^{a)}Electronic mail: sundholm@chem.helsinki.fi

theory methods. The word aromaticity is used throughout as a synonym for the ability of the molecule to sustain a magnetically induced ring current.

II. COMPUTATIONAL METHODS

The recently developed gauge-including magnetically induced current (GIMIC) method is used to explicitly calculate the strengths of the magnetically induced currents in the aluminum rings of the Al_4^{2-} and Al_4^{4-} species.¹⁶ The GIMIC method has been interfaced to the Austin–Mainz version of the ACES II (Ref. 17) and to the TURBOMOLE (Ref. 18) program packages. The first-order magnetically induced current densities have been calculated for the Al_4^{2-} and Al_4^{4-} species at the coupled-cluster singles and doubles (CCSD) level.^{19,20} Additional shielding and current-density calculations at the CCSD level augmented by a perturbative treatment of triple excitations²¹ [CCSD(T)] have been performed for Al_4Li_2 to check the reliability of the corresponding CCSD results. In the GIMIC method, gauge-including atomic orbitals^{22–26} (GIAOs) were employed yielding gauge-origin independent current densities with a fast basis-set convergence; standard basis sets give current densities close to the basis-set limit rendering GIMIC calculations on large molecules feasible.¹⁶ GIMIC calculations can be performed at any computational level for which the one-body density matrix and the magnetically perturbed density matrices are available.^{20,21,25–36} The GIMIC method and its implementation have been described in Ref. 16.

In the nuclear magnetic shielding calculations at the coupled-cluster and HF SCF levels, the Karlsruhe triple-zeta quality basis sets augmented with polarization functions (TZP) were employed.¹⁸ The molecular structures used in the *ab initio* GIMIC calculations were optimized at the CCSD/TZP level. Since, we are mainly interested in a qualitative treatment of the electron-correlation effects, calculations at the CCSD level are sufficiently accurate. A comparison of CCSD/TZP results with the results obtained at the CCSD level using split-valence quality (SVP) basis sets³⁷ (not reported) showed that CCSD/TZP calculations are adequate for this purpose.

The nuclear magnetic shielding calculations provide the magnetically perturbed density matrices which are used in the calculation of the magnetically induced current density. The strength of the induced ring currents was obtained by performing a numerical integration of the induced current density passing through a cross section perpendicular to chemical bonds of the molecular ring.¹⁶

For a fixed direction of the external magnetic field, the magnetically induced current density is a vector function with length and direction. This means that the magnetically induced currents *per se* cannot be classified as diatropic or paratropic. However, by introducing a reference frame, in this case the integration cross-section plane, the sign of the perpendicular projection of the current density against this plane defines whether the current-density function is diatropic or paratropic in the cross-section plane. This can be considered to be related to the evaluation of the paramagnetic contribution to the nuclear magnetic shielding constants

needed in the calculation of magnetic spin-rotation constants.³⁸

In the DFT calculations of the nuclear magnetic shieldings, the molecular structures were optimized using Becke's three-parameter functional for exchange in combination with the Lee–Yang–Parr correlation functional^{39,40} (B3LYP) and the Karlsruhe triple-zeta valence polarization (TZVP) quality basis sets.⁴¹ The nuclear magnetic shieldings were also calculated at the B3LYP/TZVP level.

The aromatic ring-current shieldings (ARCSs)⁴² and NICSs were also calculated at the CCSD/TZP and B3LYP/TZVP levels. The diatropic or paratropic character of the magnetically induced ring-current susceptibility was estimated from the long-range part of the ARCS function, i.e., the magnetic shielding function calculated along a line from the ring center and perpendicular to the ring as described in our previous work.^{10,42–46} For comparison, we also report NICS values⁴ calculated at the CCSD/TZP and B3LYP/TZVP levels.

III. MOLECULAR STRUCTURES

The molecular structures optimized at the CCSD/TZP level are shown in Fig. 1. The Al–Al bond distances obtained in the CCSD/TZP and B3LYP/TZVP calculations are given in Table I. The molecular structures obtained at the B3LYP/TZVP and CCSD/TZP levels are very similar; the Al–Al distances differ by less than 2 pm. In the case of Al_4Li_2 , B3LYP provides a symmetry-broken structure with the Li atoms connected to only two of the Al atoms. The distances between the axial Li atoms and the ring center calculated at the B3LYP/TZVP and CCSD/TZP levels differ by 4 pm, except for Al_4Li_2 .

IV. NICS CALCULATIONS

The NICS value, which is often used to probe the strength of the magnetically induced ring current, is defined as the negative value of the isotropic magnetic shielding at the ring center.⁴ This commonly used molecular aromaticity index⁴⁶ has recently met harsh criticism.⁴⁷ The NICS index is employed here for comparison, since Chen *et al.*³ used it in their study of the aromaticity of Al_4^{4-} . A negative NICS value, i.e., diamagnetic (positive) shielding, corresponds to aromatic species and antiaromatic molecules exhibit positive NICS values. The NICS values of Al_4Li^- , Al_4Li_2 , Al_4Li_3^- , and Al_4Li_4 calculated at the B3LYP/TZVP level using the fully optimized B3LYP/TZVP structures are -18.2 , -1.7 , -5.9 , and -10.4 ppm, respectively. The corresponding NICS values calculated at the CCSD/TZP level using the CCSD/TZP optimized structures are -24.1 , -5.4 , -12.0 , and -16.7 ppm, suggesting that they are all aromatic. The fully optimized structure of Al_4Li_2 obtained at the B3LYP/TZVP level has a symmetry-broken structure with slightly alternating Al–Al bonds of 260.4 and 263.3 pm and with the Li atoms coordinated to only two Al atoms. The optimized CCSD/TZP structure belongs to the D_{4h} point group with

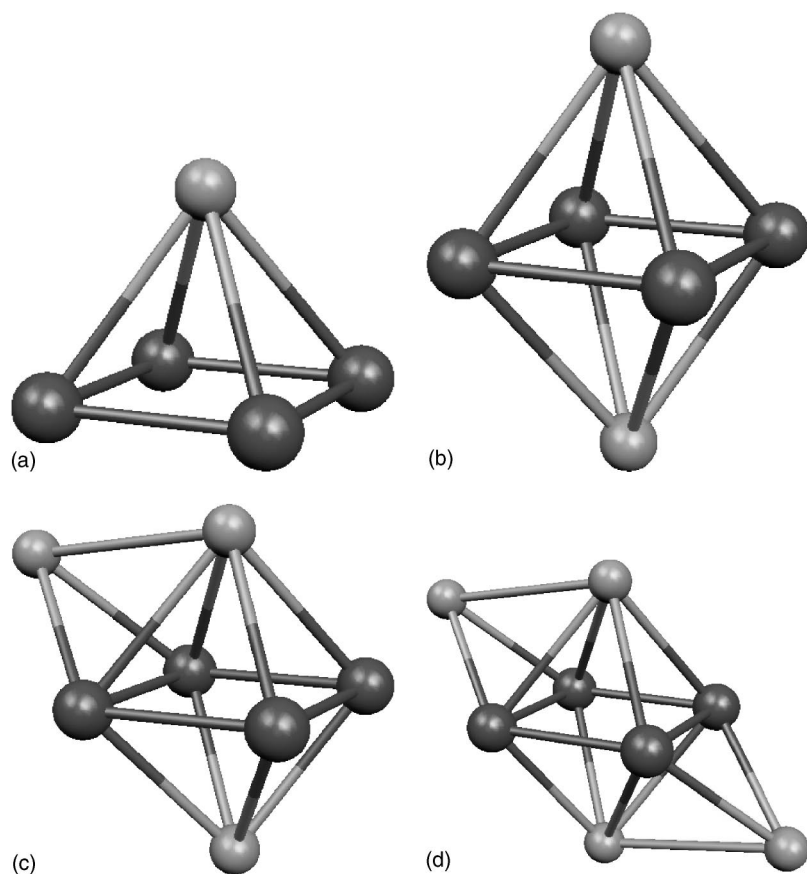


FIG. 1. The molecular structure of Al_4Li^- , Al_4Li_2 , Al_4Li_3^- , and Al_4Li_4 optimized at the CCSD/TZP level.

identical Al–Al distances. The NICS value for Al_4Li_2 calculated at the B3LYP/TZVP level using the D_{4h} structure is 15.5 ppm, indicating that it is antiaromatic, whereas the NICS value obtained at the B3LYP/TZVP level using the symmetry-broken structure is -1.7 ppm as compared with the CCSD/TZP value of -5.4 ppm. Thus, Al_4Li_2 is indeed a complicated system that must be studied at highly correlated levels of theory.

The large difference of a factor of 10 between the NICS values calculated for Al_4Li^- and Al_4Li_2 at the B3LYP/TZVP level and the corresponding ratio of 4 obtained at the CCSD/TZP level are somewhat distressing because the structural

difference between the two species is mainly due to the different number of Li^+ cations surrounding the Al_4^{2-} ring. For ionic systems such as these species, the number of counterions should not significantly affect the aromaticity properties of the Al_4 ring. For the two Al_4^{4-} species, the NICS values calculated at the B3LYP/TZVP level differ by a factor of 2. At the CCSD/TZP level, the NICS values for the two Al_4^{4-} species differ by 6 ppm. The NICS value does not seem to be a reliable aromaticity index, since the B3LYP and CCSD NICS values give completely different notions about the degree of aromaticity of the Al_4 rings. The approximately constant difference between the NICS values calculated at the

TABLE I. The Al–Al bond distances (in pm) of the Al_4 species optimized at the CCSD and B3LYP levels. The distance between the ring center and the axial Li cations ($R_c\text{--Li}$ in pm) are also given.

Species	Level	Symmetry	Al–Al	Al–Al	$R_c\text{--Li}$
Al_4Li^-	B3LYP/TZVP	C_{4v}	261	...	220
Al_4Li^-	CCSD/TZP	C_{4v}	259	...	226
Al_4Li_2	B3LYP/TZVP	C_{2h}	260	263	230
Al_4Li_2	B3LYP/TZVP	D_{4h}	263	...	223
Al_4Li_2	CCSD/TZP	D_{4h}	261	...	230
Al_4Li_3^-	B3LYP/TZVP	C_s	250	257 ^a	204 ^b
Al_4Li_3^-	CCSD/TZP	C_s	249	257 ^c	208 ^b
Al_4Li_4	B3LYP/TZVP	C_{2h}	255	267	214
Al_4Li_4	CCSD/TZP	C_{2h}	255	269	218

^aThe two other Al–Al bond distances are 279 pm.

^bAt the B3LYP/TZVP level, the axial $R_c\text{--Li}$ distance on the side with two Li atoms is 211 pm and at the CCSD/TZP level it is 216 pm.

^cThe two other Al–Al bond distances are 277 pm.

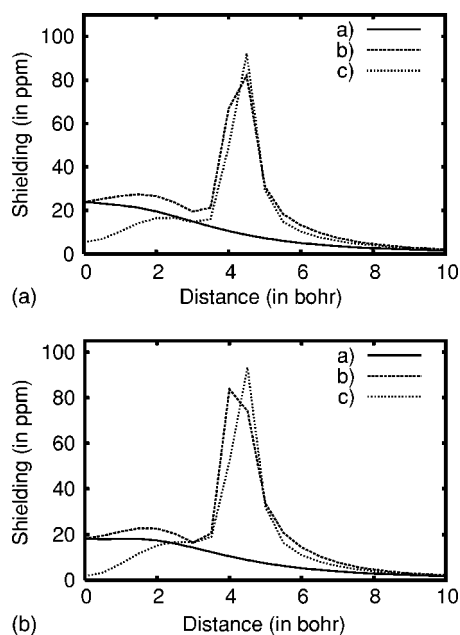


FIG. 2. The ARCS functions (in ppm) for the Al_4^{2-} species calculated at the CCSD/TZP (upper) and B3LYP/TZVP (lower) levels. (a) For Al_4Li^- , calculated on the open side of the Al_4 ring. (b) For Al_4Li^- , calculated on the other side of the Al_4 ring. (c) Calculated for Al_4Li_2 .

B3LYP and CCSD levels is due to the well-known fact that magnetic shieldings are often systematically underestimated at DFT levels of theory.⁴⁸

V. ARCS CALCULATIONS

An alternative approach to estimate the degree of aromaticity is the ARCS method which deduces the degree of aromaticity from the long-range magnetic shielding function.⁴² For simple ring-shaped molecules, the ARCS function also can provide estimates for the strength of the induced ring current by employing Biot–Savart’s law for an infinitely thin ring.⁴³

The ARCS functions for the Al_4^{2-} and Al_4^{4-} species calculated at the CCSD/TZP and B3LYP/TZVP levels are shown in Figs. 2 and 3. In a previous study, ARCS calculations at the CCSD level gave ring-current susceptibilities of 11.6 and 11.9 nA/T for Al_4^{2-} and Al_4Li^- , respectively.¹⁰ These values can be compared to the present value of 28.1 nA/T for Al_4Li^- obtained at the CCSD/TZP level by numerical integration of the current density. The current strengths obtained from the ARCS calculations are underestimated by about a factor of 2, since for the Al_4 species the assumption that the ring current is circular, infinitely thin, and circling in the Al_4 plane is a rather crude approximation. For Al_4Li_2 , Al_4Li_3^- , and Al_4Li_4 , a quantitative determination of the ring-current susceptibility from ARCS functions is more complicated, since the counterions above the ring center interfere with the ARCS fit.

The sign and shape of the ARCS function at long distances from the Al_4 ring show whether the molecule possesses dominating diamagnetic or paramagnetic character. As seen in Fig. 2, the positive tail of the shielding functions indicates that the Al_4Li^- and Al_4Li_2 rings sustain net diatropic currents, whereas Al_4Li_3^- and Al_4Li_4 seem to be domi-

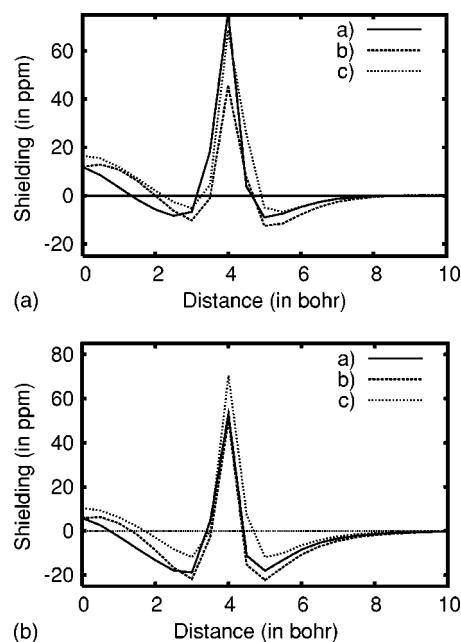


FIG. 3. The ARCS functions (in ppm) for the Al_4^{4-} species calculated at the CCSD/TZP (upper) and B3LYP/TZVP (lower) levels. (a) The ARCS function on the side of Al_4Li_3^- with one Li^+ cation less than in case (b). (c) The ARCS function for Al_4Li_4 .

nated by paratropic currents. However, at very long distances (more than 15 bohrs from the Al_4 ring), the shielding changes sign and become diamagnetic for both Al_4^{4-} species. The inner part and the distant parts of the ARCS function suggest that in Al_4^{4-} diatropic and paratropic currents play an important role, rendering an unambiguous interpretation of the ARCS function difficult. In Sec. VI, we show that GIMIC calculations can assist the interpretation of the shape of the ARCS function and provide a plausible explanation of its asymptotic behavior at long distances.

VI. GIMIC CALCULATIONS

A. Al_4^{2-} and Al_4^{4-}

The first-order magnetically induced current densities calculated for the Al_4^{2-} and Al_4^{4-} compounds at the CCSD/TZP level using the GIMIC method verify the earlier notion^{5,6} that both aluminum rings sustain strong diatropic currents in the Al_4 plane. For the Al_4^{2-} species, the induced currents at distances of 1.5–3.5 bohrs above and below the Al_4 ring are also characterized by diatropic currents. The Al_4^{4-} species have strong paratropic currents in the same π region, whereas diatropic currents are sustained in the σ orbitals, i.e., up to 1.5 bohrs above (below) the ring plane. Thus, based on these observations, one might claim that the Al_4^{2-} species are both σ and π aromatic, whereas the Al_4^{4-} species are σ aromatic and π antiaromatic.

It is hard to extract any accurate quantitative information from current-density plots (not shown). A more quantitative analysis can be obtained by performing numerical integrations¹⁶ of the current densities passing through a cross section perpendicular to the Al–Al bonds, as shown in Fig. 4. Quantitative values for the diatropic and paratropic contributions to the ring currents can be obtained by integrating them

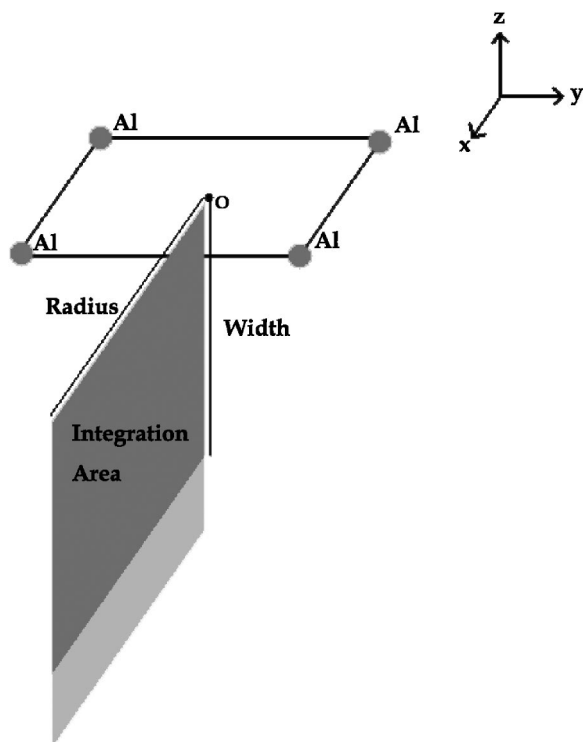


FIG. 4. The integration cross section used in the calculation of the integrated current-density distributions.

separately, i.e., separating the positive and negative contributions to the total current. The diatropic currents are here defined as the positive currents.

Detailed information about the spatial distribution of the ring current can be deduced from the two-dimensional distribution function showing the current contributions passing the cross section. A more convenient representation is given by one-dimensional distribution functions obtained by integration of the two-dimensional current distribution in one of the two dimensions (width or radius). The perpendicular distance from the ring is here denoted as the width (see Fig. 4). Thus, the “width distribution function” is the radially integrated current as a function of the distance from the molecular plane. Analogously, the “radial distribution function” is obtained by integrating along the width coordinate. For interpretation of the currents, a better representation is given by the ring-current “shape function,” calculated as the first derivative of the radial distribution functions with respect to the radial distance from the ring center.

The current strengths given in Table II are obtained using quadrature. The integrated current strengths also include contributions from the currents around the Li cations above and below the ring center, and are therefore not an exact measure of the *ring-current* strength. The strength of the Li⁺ currents can be estimated by comparing the integrated current functions of Al₄Li⁻ with Al₄Li₂. The Li⁺ currents in Al₄Li₃⁻ and Al₄Li₄ were obtained by integrating the current susceptibility in the vicinity of the Li atom. The estimated Li⁺ contributions are 4.3 and 2.4 nA/T for the Al₄²⁻ and Al₄⁴⁻ species, respectively. The integrated ring-current susceptibilities of the Al₄ rings in the Al₄Li⁻, Al₄Li₂, Al₄Li₃⁻, and Al₄Li₄ species then become 28.1, 28.1, -5.9, and -3.1 nA/T,

TABLE II. The integrated ring-current susceptibilities (in nA/T) for the Al₄ species calculated at the CCSD/TZP level using the GIMIC method.

	Al ₄ Li ⁻	Al ₄ Li ₂	Al ₄ Li ₃ ^{-a}	Al ₄ Li ₄
Diamagnetic current	32.4	36.7	18.9	18.6
Paramagnetic current	0.0	0.0	-19.9	-16.8
Total current	32.4	36.7	-1.0	1.8
Contribution from Li ^b	4.3	8.6	4.9	4.9
Total ring current	28.1	28.1	-5.9	-3.1

^aThe current passing the two identical Al–Al bonds are given in the table. The corresponding values for the shortest Al–Al bond are 22.4, -23.6, -1.3, 4.9, and -6.2 nA/T, respectively.

^bThe estimated net current circling the Li⁺ cations. For Al₄²⁻, the current around Li⁺ is estimated from the two halves of Al₄Li⁻. For the Al₄⁴⁻ species, the Li current is obtained by integration of the current contributions in the vicinity of the ring center and outside 3.5 bohrs from the Al-ring plane.

respectively. Thus Al₄²⁻ can be considered aromatic, whereas according to the same criterion the Al₄⁴⁻ species are more or less nonaromatic or possibly weakly antiaromatic; the ring-current susceptibility of benzene calculated at the CCSD/TZP level is 11.8 nA/T.¹⁶

In Fig. 5, one can see that strong diatropic currents are sustained in the σ orbitals of Al₄Li₂, but about half the current (20 nA/T) originates from spatial positions which are more than 1.5 bohrs above (and below) the Al₄ plane, including the Li⁺ cations; the σ and the π densities are about equally responsible for the ring current in Al₄²⁻. The total ring currents for Al₄Li⁻ and Al₄Li₂ are completely dominated by positive contributions indicating that they are aromatic species. The calculated ring-current susceptibilities of Al₄Li⁻ and Al₄Li₂ are identical, showing that the Li⁺ counterions form largely ionic bonds to the Al₄²⁻ ring. The large discrepancy between the NICS values obtained for Al₄Li⁻ and Al₄Li₂ is thus not a result of differences in the strength of the ring currents but must be due to some other reason casting shadows on the reliability of the NICS route to molecular aromaticity.

A comparison of the curves in Figs. 5 and 6 shows that at 1.5 bohrs, the integrated diatropic contribution in the Al₄⁴⁻ species is 26% smaller than for Al₄²⁻ and the paratropic contribution in Al₄Li₄ is only 4% of the diatropic current. In Fig. 6 one can see that Al₄Li₃⁻ and Al₄Li₄ sustain significant diatropic and paratropic currents of about equal size, indicating that they are practically nonaromatic or slightly antiaromatic. On the other hand, the ARCS calculations show that

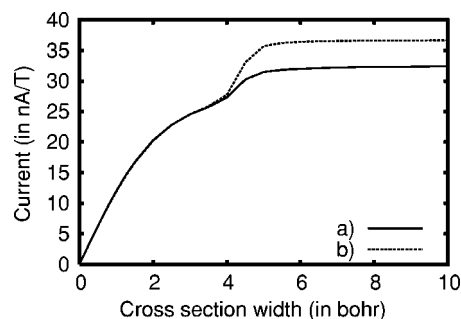


FIG. 5. The integrated current densities for (a) Al₄Li⁻ and (b) Al₄Li₂ calculated at the CCSD/TZP level given as a function of the width of the integration cross section as defined in Fig. 4.

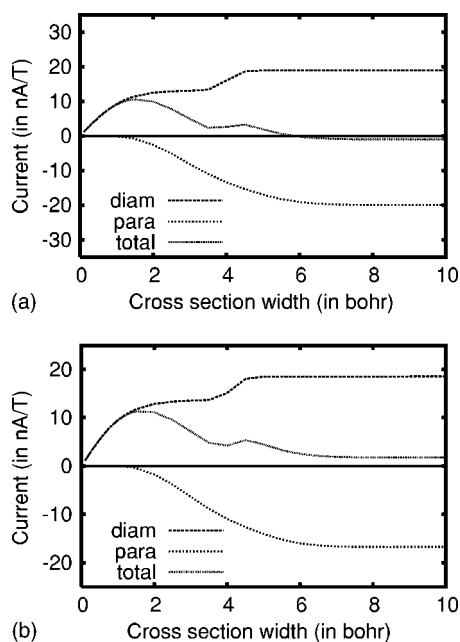


FIG. 6. The integrated current densities for Al_4Li_3^- (upper) and Al_4Li_4 (lower) calculated at the CCSD/TZP level given as a function of the width of the integration cross section as defined in Fig. 4. The diatropic and paratropic contributions are also shown.

the ring currents in the Al_4^{4+} species give rise to diamagnetic shieldings distant from the molecular ring. Thus, even though the strength of the net ring current in the Al_4^{4+} species is close to zero as shown by the GIMIC calculations, the molecule possesses a significant magnetic shielding at long distances from the Al_4 ring outside the electron density. For nonaromatic molecules, the magnetic shielding declines fast with the distance to the ring and for them practically no magnetic shieldings appear outside the charge density. Thus according to these criteria, the Al_4^{4+} species are neither aromatic, antiaromatic, nor nonaromatic. Instead, the Al_4^{4+} species can be considered to belong to a new class of molecules with the peculiar property of having long-range magnetic shieldings without sustaining any strong net ring current. Another member of this class of molecules is C_{60} which has recently been shown to sustain strong diatropic and paratropic spherical currents that almost completely cancel.⁴⁹ For this class of molecules, the long-range magnetic shielding does not vanish, because the average radii of the diatropic

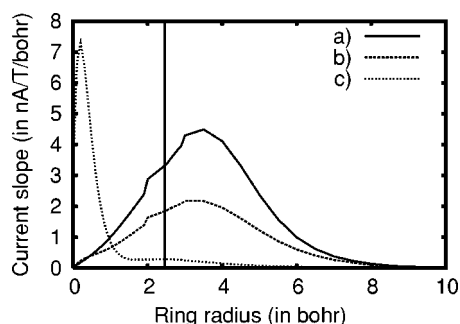


FIG. 7. The ring-current profiles for Al_4Li^- calculated at the CCSD/TZP level. The integration intervals (in bohr) in the width direction are (a) $[-1.5, 1.5]$, (b) $[-3.5, -1.5] + [1.5, 3.5]$, and (c) $[-10.0, -3.5] + [3.5, 10.0]$, representing the σ density, the π density, and the rest.

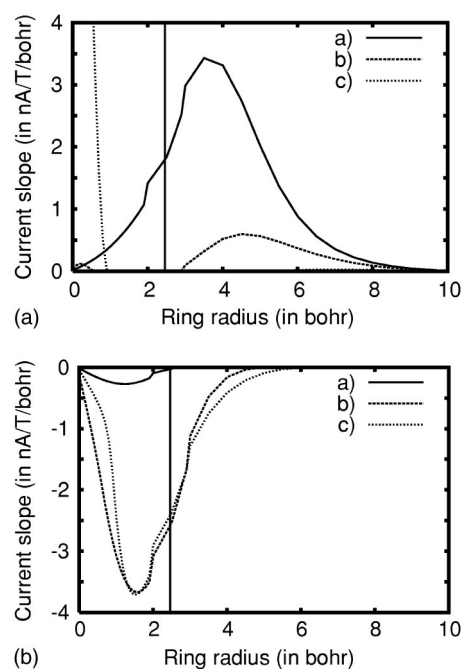


FIG. 8. The diatropic (upper) and paratropic (lower) current-density profiles for Al_4Li_4 calculated at the CCSD/TZP level. The integration intervals (in bohr) in the width direction are (a) $[-1.5, 1.5]$, (b) $[-3.5, -1.5] + [1.5, 3.5]$, and (c) $[-10.0, -3.5] + [3.5, 10.0]$ representing the σ density, the π density, and the rest.

and paratropic currents are different. The current with the largest radius characterizes the magnetic shieldings at very long distances.

The ring-current profiles for Al_4Li^- calculated at the CCSD/TZP level are shown in Fig. 7. In the integration of the ring-current profiles, the width has been divided into three regions: (1) $[-1.5, 1.5]$ bohrs, where σ currents are expected; (2) π currents are mainly sustained in the $[-3.5, -1.5]$ and $[1.5, 3.5]$ intervals; (3) in the $[-10.0, -3.5]$ and $[3.5, 10.0]$ intervals the Li^+ currents and current contributions from very diffuse orbitals appear. For Al_4Li^- , the integrated ring-current contributions from these regions are 16.7, 9.0, and 6.6 nA/T. The corresponding graphs for Al_4Li_4 are shown in Fig. 8. In this case, the integrated ring-current contributions from the three regions are 11.8 (−0.4), 1.9 (−8.4), and 4.9 (−7.9) nA/T, respectively. The paratropic contributions are given in parentheses. The paratropic contribution

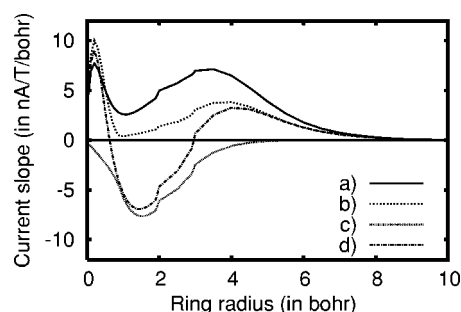


FIG. 9. A comparison of the radial ring-current distribution functions for Al_4Li^- and Al_4Li_4 calculated at the CCSD/TZP level. (a) The diatropic (and total) current for Al_4Li^- . (b) The diatropic current for Al_4Li_4 . (c) The paratropic current for Al_4Li_4 . (d) The net ring-current distribution for Al_4Li_4 .

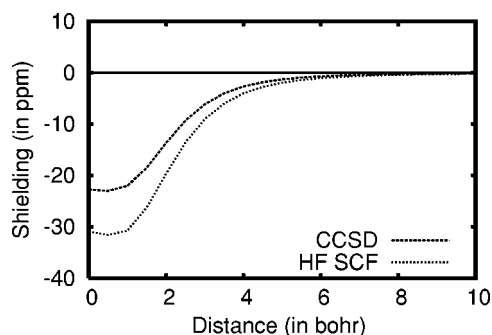


FIG. 10. The ARCS function for C_4H_4 (in ppm) calculated at the CCSD/TZP and HF SCF/TZP levels.

from the vicinity of the Al_4 ring is small; the size of the tiny paratropic contribution seen in Fig. 8 originates from the π orbitals and its magnitude depends on the exact position of the chosen border line between σ and π densities. The paratropic contribution is almost equally divided between the π density in the interval [1.5,3.5] and the outer regions of the molecule showing the presence of strong paratropic currents in the diffuse part of the electron density.

Figure 7 shows that for Al_4Li_2 the average radii of the σ and π currents are equal. The peak at small radii is due to Li^+ . The graphs in Figs. 8 and 9 reveal that the average size of the paratropic currents is somewhat smaller than the Al_4Li_4 ring and that the σ current is sustained in the p_σ orbitals as for Al_4Li_2 . The paratropic currents appear at significantly larger width distances from the ring than the diatropic one. The larger radius of the diatropic current results in a dominating diamagnetic character of the tail of the long-range magnetic shielding function; the ARCS function at large distances from the Al_4 ring is positive. The negative ARCS function between 6 and 10 bohrs is due to the dominating paratropic currents with a smaller effective radius than for the diatropic one. The current distribution functions in Fig. 9 explain the obtained shape of the ARCS function for the Al_4^{4-} species.

B. C_4H_4

The magnetically induced currents were also calculated for cyclobutadiene, which is the archetypical antiaromatic molecule. The ARCS function is given in Fig. 10 and the integrated current strength as a function of the distance from the ring plane (width) is shown in Fig. 11. The ARCS and GIMIC calculations show that paratropic currents are induced in the π orbitals of C_4H_4 . The net ring-current susceptibility calculated at the CCSD/TZP level for C_4H_4 is about -18 nA/T. The C_4H_4 molecule sustains strong paratropic currents in the π orbitals, but some paratropic currents are also induced in the σ orbitals. However, the paratropic σ current is to some extent canceled by the diatropic σ current, the strength of which is about 4 nA/T.

VII. NUCLEAR MAGNETIC SHIELDING CALCULATIONS

The ^{27}Al nuclear magnetic shielding, $\sigma(^{27}Al)$, calculated for the Al_4 species are given in Table III. The calculations

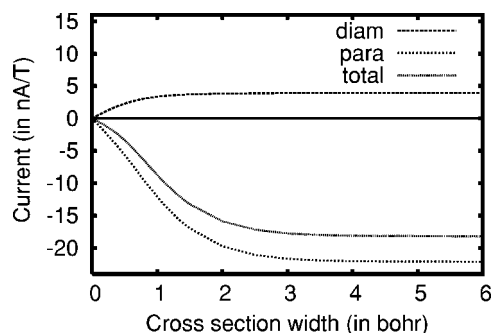


FIG. 11. The integrated current densities for C_4H_4 calculated at the CCSD/TZP level given as a function of the width of the integration cross section of the formal double bond as defined in Fig. 4. The diatropic and paratropic contributions are also shown.

show that $\sigma(^{27}Al)$ is strongly dependent on the level of correlation treatment, the number of Li^+ counterions, and the formal charge of the Al_4 ring. For Al_4Li^- , the HF SCF/TZP and B3LYP/TZP shieldings are 35 and 45 ppm, respectively, which can be compared to the CCSD/TZP value of 198 ppm. The ^{27}Al shielding of Al_4Li_2 calculated at the CCSD/TZP level is -99 ppm and by considering also triple excitations, it becomes -95 ppm. At the HF SCF/TZP level, the ^{27}Al shielding of Al_4Li_2 is -647 ppm. The correlation contribution calculated at the CCSD/TZP level is about 550 ppm, whereas the triple excitations have almost no effect on the ^{27}Al nuclear magnetic shielding constants. The B3LYP/TZVP value of -527 ppm obtained using the D_{4h} structure is close to the HF SCF/TZP value. However, the $\sigma(^{27}Al)$ value calculated at the B3LYP/TZVP level for the fully optimized B3LYP/TZVP structure (D_{2h}) is -270 ppm. The symmetry breaking of the molecular structure results in a huge change

TABLE III. The nuclear magnetic shieldings (in ppm) for the Al_4 species calculated at the HF SCF/TZP, B3LYP/TZVP, and CCSD/TZP levels. For Al_4Li_2 , the nuclear magnetic shieldings calculated at the CCSD(T) level are also given. In the HF SCF, CCSD, and CCSD(T) shielding calculations, the molecular structures were optimized at the CCSD/TZP level. In the B3LYP/TZVP shielding calculations, the molecular structures optimized at the B3LYP/TZVP level were used.

Species	Level	$\sigma(Al)$	$\sigma(Al)$
Al_4Li^-	HF SCF/TZP	35	...
Al_4Li^-	B3LYP/TZVP	45	...
Al_4Li^-	CCSD/TZP	198	...
Al_4Li_2	HF SCF/TZP	-647	...
Al_4Li_2	B3LYP/TZVP	-527^a	...
Al_4Li_2	B3LYP/TZVP	-270	-271^b
Al_4Li_2	CCSD/TZP	-99	...
Al_4Li_2	CCSD(T)/TZP	-95	...
$Al_4Li_3^-$	HF SCF/TZP	200 ^c	304
$Al_4Li_3^-$	B3LYP/TZVP	249 ^c	360
$Al_4Li_3^-$	CCSD/TZP	363 ^c	474
Al_4Li_4	HF SCF/TZP	238	...
Al_4Li_4	B3LYP/TZVP	273	...
Al_4Li_4	CCSD/TZP	413	...

^aThe D_{4h} symmetry was assumed.

^bCalculated in C_1 (C_{2h}) symmetry. The magnetic shieldings of the two other Al nuclei are -270 and -268 ppm.

^cFor the Al atoms closer to Li at the edge.

of 280 ppm for $\sigma(^{27}\text{Al})$, showing again the importance of an adequate treatment of the electron-correlation effects for Al_4Li_2 .

The substantial difference of 300 ppm between the ^{27}Al shieldings of Al_4Li_2 and Al_4Li^- obtained at the CCSD/TZP level is also remarkable, since formally the only difference between these species is the number of Li^+ counterions. In contrast, the ^{27}Al shieldings of Al_4Li_3^- and Al_4Li_4 calculated at the CCSD/TZP level differ by 50–60 ppm, which is closer to the expected size of the counterion effects.

The CCSD/TZP lithium shieldings, $\sigma(^7\text{Li})$, for Al_4Li^- and Al_4Li_2 calculated at the CCSD/TZP level are 112.9 and 108.6 ppm, whereas at the HF SCF/TZP level they are 117.5 and 119.2 ppm. These values can be compared to the $\sigma(^7\text{Li})$ value of 95.4 ppm obtained at the HF SCF/TZP level for a single Li^+ cation.

VIII. CONCLUSIONS

The present GIMIC calculations performed at the CCSD/TZP level show that the electrons in both the σ and π orbitals are responsible for the transport of the magnetically induced ring currents in Al_4^{2-} and Al_4^{4-} rings. In Al_4^{2-} , the σ and π orbitals sustain merely diatropic currents of 16.7 and 11.3 nA/T, respectively. When one relates diatropic currents to aromaticity, one can claim that Al_4^{2-} is simultaneously σ and π aromatic.

In Al_4^{4-} , the spatial distribution of the integrated diatropic current looks similar to that of Al_4^{2-} . The Al_4^{4-} species have a slightly weaker σ current of 14 nA/T, whereas for these species the π orbitals sustain strong paratropic currents of about -17 nA/T, yielding an almost vanishingly small ring-current susceptibility, suggesting that the Al_4^{4-} species are nonaromatic or slightly antiaromatic. The spatial distributions of the induced diatropic and paratropic currents are significantly different, resulting in nonzero long-range magnetic shieldings as observed for both aromatic and antiaromatic species. Thus, when relating the diatropic and paratropic currents to aromaticity and antiaromaticity, Al_4^{4-} can in a sense be considered simultaneously σ aromatic and π antiaromatic, as previously suggested by Chen *et al.*³ and by Fowler and co-workers.^{5,6} The Al_4^{4-} species can be considered to belong to a new class of molecules with the peculiar property of having long-range magnetic shieldings without sustaining any strong net ring current. Even though the net ring current is dominated by paratropic contributions, the tail of the long-range magnetic shielding function is diatropic because the current radius of the diatropic current is slightly larger than the radius of the paratropic one. The present study also shows that NICS values are not an accurate indicator for the molecular aromaticity of these cage-shaped molecules.

ACKNOWLEDGMENTS

We acknowledge financial support from the European research training network on “Understanding Nanomaterials from a Quantum Perspective (NANOQUANT),” Contract No. MRTN-CT-2003-506842, from the Nordisk Forskerakademikernet for research and research training (NorFA Grant No. 030262) on “Quantum Modeling of Molecular

Materials” (QMMM), from the Academy of Finland (FA projects 53915, 200903, and 206102), from Magnus Ehrnrooth’s Foundation, the BMBF “Zentrum für multifunktionelle Werkstoffe und miniaturisierte Funktionseinheiten,” the “Deutsche Forschungsgemeinschaft,” and the “Fonds der Chemischen Industrie.” One of the authors (J.J.) has been a member of the graduate school LASKEMO financed by the Ministry of Education, Finland. We also thank Professor Reinhart Ahlrichs (Karlsruhe) for an up-to-date version of the TURBOMOLE program package.

- ¹X. Li, A. E. Kuznetsov, H.-F. Zhang, A. I. Boldyrev, and L.-S. Wang, *Science* **291**, 859 (2001).
- ²A. E. Kuznetsov, K. A. Birch, A. I. Boldyrev, X. Li, H.-J. Zhai, and L.-S. Wang, *Science* **300**, 622 (2003).
- ³Z. Chen, C. Corminboeuf, T. Heine, J. Bohmann, and P. von Ragué Schleyer, *J. Am. Chem. Soc.* **125**, 13930 (2003).
- ⁴P. von Ragué Schleyer, C. Maerker, A. Dransfeld, H. Jiao, and N. J. R. van Eikema Hommes, *J. Am. Chem. Soc.* **118**, 6317 (1996).
- ⁵P. W. Fowler, R. W. A. Havenith, and E. Steiner, *Chem. Phys. Lett.* **342**, 85 (2001).
- ⁶R. W. A. Havenith, P. W. Fowler, E. Steiner, S. Shetty, D. Kanhere, and S. Pal, *Phys. Chem. Chem. Phys.* **6**, 285 (2004).
- ⁷S. K. Ritter, *Chem. Eng. News* **81**, 23 (2003).
- ⁸A. E. Kuznetsov, A. I. Boldyrev, X. Li, and L.-S. Wang, *J. Am. Chem. Soc.* **123**, 8825 (2001).
- ⁹A. E. Kuznetsov, J. D. Corbett, L.-S. Wang, and A. I. Boldyrev, *Angew. Chem., Int. Ed.* **40**, 3369 (2001).
- ¹⁰J. Jusélius, M. Straka, and D. Sundholm, *J. Phys. Chem. A* **105**, 9939 (2001).
- ¹¹J. C. Santos, J. Andres, A. Aizman, and P. Fuentealba, *J. Chem. Theory Comput.* **1**, 83 (2005).
- ¹²A. Datta and S. K. Pati, *J. Phys. Chem. A* **108**, 9527 (2004).
- ¹³A. I. Boldyrev and A. E. Kuznetsov, *Inorg. Chem.* **41**, 532 (2002).
- ¹⁴C.-G. Zhan, F. Zheng, and D. A. Dixon, *J. Am. Chem. Soc.* **124**, 14795 (2002).
- ¹⁵A. Datta and S. K. Pati, *J. Am. Chem. Soc.* **127**, 3496 (2005).
- ¹⁶J. Jusélius, D. Sundholm, and J. Gauss, *J. Chem. Phys.* **121**, 3952 (2004).
- ¹⁷J. F. Stanton, J. Gauss, J. D. Watts, W. J. Lauderdale, and R. J. Bartlett, *Int. J. Quantum Chem., Symp.* **26**, 879 (1992); current version: see <http://www.aces2.de>
- ¹⁸R. Ahlrichs, M. Bär, M. Häser, H. Horn, and C. Kölmel, *Chem. Phys. Lett.* **162**, 165 (1989); current version: see <http://www.turbomole.de>
- ¹⁹G. D. Purvis and R. J. Bartlett, *J. Chem. Phys.* **76**, 1910 (1982).
- ²⁰J. Gauss and J. F. Stanton, *J. Chem. Phys.* **102**, 251 (1995).
- ²¹J. Gauss and J. F. Stanton, *J. Chem. Phys.* **104**, 2574 (1996).
- ²²F. London, *J. Phys. Radium* **8**, 397 (1937).
- ²³H. Hameka, *Mol. Phys.* **1**, 203 (1958).
- ²⁴R. Ditchfield, *Mol. Phys.* **27**, 789 (1974).
- ²⁵P. Pulay, J. F. Hinton, and K. Wolinski, in *Nuclear Magnetic Shieldings and Molecular Structure*, NATO Advanced Studies Institute, Series C: Mathematical and Physical Sciences, edited by J. A. Tossell (Kluwer, Dordrecht, 1993), Vol. 386, p. 243.
- ²⁶K. Wolinski, J. F. Hinton, and P. Pulay, *J. Am. Chem. Soc.* **112**, 8251 (1990).
- ²⁷M. Häser, R. Ahlrichs, H. P. Baron, P. Weis, and H. Horn, *Theor. Chim. Acta* **83**, 551 (1992).
- ²⁸J. Gauss, *Chem. Phys. Lett.* **191**, 614 (1992).
- ²⁹J. Gauss, *J. Chem. Phys.* **99**, 3629 (1993).
- ³⁰K. Ruud, T. Helgaker, R. Kobayashi, P. Jørgensen, K. L. Bak, and H. J. Aa. Jensen, *J. Chem. Phys.* **100**, 8178 (1994).
- ³¹A. M. Lee, N. C. Handy, and S. M. Colwell, *J. Chem. Phys.* **103**, 10095 (1995).
- ³²G. Schreckenbach and T. Ziegler, *J. Phys. Chem.* **99**, 606 (1995).
- ³³J. R. Cheeseman, G. W. Trucks, T. A. Keith, and M. J. Frisch, *J. Chem. Phys.* **104**, 5497 (1996).
- ³⁴G. Rauhut, S. Puyear, K. Wolinski, and P. Pulay, *J. Phys. Chem.* **100**, 6310 (1996).
- ³⁵J. Gauss, *J. Chem. Phys.* **116**, 4773 (2002).
- ³⁶M. Kállay and J. Gauss, *J. Chem. Phys.* **120**, 6841 (2004).
- ³⁷A. Schäfer, H. Horn, and R. Ahlrichs, *J. Chem. Phys.* **97**, 2571 (1992).
- ³⁸J. Gauss, K. Ruud, and T. Helgaker, *J. Chem. Phys.* **105**, 2804 (1996).

- ³⁹A. D. Becke, J. Chem. Phys. **98**, 5648 (1993).
- ⁴⁰C. Lee, W. Yang, and R. G. Parr, Phys. Rev. B **37**, 785 (1988).
- ⁴¹A. Schäfer, C. Huber, and R. Ahlrichs, J. Chem. Phys. **100**, 5829 (1994).
- ⁴²J. Jusélius and D. Sundholm, Phys. Chem. Chem. Phys. **1**, 3429 (1999).
- ⁴³J. Jusélius and D. Sundholm, Phys. Chem. Chem. Phys. **2**, 2145 (2000).
- ⁴⁴R. J. F. Berger, M. A. Schmidt, J. Jusélius, D. Sundholm, P. Sirsch, and H. Schmidbaur, Z. Naturforsch., B: Chem. Sci. **56**, 979 (2001).
- ⁴⁵J. Jusélius, M. Patzschke, and D. Sundholm, J. Mol. Struct.: THEOCHEM **633**, 123 (2003).
- ⁴⁶Z. Chen, T. Heine, D. Sundholm, and P. von Ragué Schleyer, in *Quantum Chemical Calculation of Magnetic Resonance Properties*, edited by M. Kaupp, M. Bühl, and V. Malkin (Wiley, Weinheim, 2004), pp. 395–407.
- ⁴⁷P. Lazzaretti, Phys. Chem. Chem. Phys. **6**, 217 (2004).
- ⁴⁸A. A. Auer, J. Gauss, and J. F. Stanton, J. Chem. Phys. **118**, 10407 (2003).
- ⁴⁹M. P. Johansson, J. Jusélius, and D. Sundholm, Angew. Chem., Int. Ed. **44**, 1843 (2005).